nature geoscience

Article

https://doi.org/10.1038/s41561-026-01929-y

# An intermittent dynamo linked to high-titanium volcanism on the Moon

Received: 28 September 2024

Accepted: 23 January 2026

Published online: 26 February 2026

Check for updates

Claire I. O. Nichols ✉, Jon Wade & Simon N. Stephenson

The history of the lunar magnetic field is a longstanding controversy. Many palaeomagnetic studies provide evidence for either a persistent, weak magnetic field or the lack of an intrinsic magnetic field between 1.020 and 3.580 billion years ago. However, for the period between 3.580 and 3.854 billion years ago, palaeomagnetic studies have recovered strong intrinsic fields (>40 μT) distributed among weak or null intensity measurements. Crustal magnetic anomalies from this period have also been interpreted as evidence for the presence of both strong and weak magnetic fields. Here we explore potential links between published palaeointensity, rock magnetic and geochemical data for lunar basalts. We find there is a statistically significant relationship only between recovered palaeointensity and the titanium content of lunar basalts. By modelling the heat flux across the core–mantle boundary, we suggest that there is a causal link between lunar dynamo generation and the eruption of high-titanium basalts. Such a link may result from the intermittent melting of ilmenite-bearing cumulates at the core–mantle boundary. The coincidence of these rare events probably reflects sampling bias near high-titanium basaltic terranes.

Models of the lunar dynamo that span the period from 3.580 to 3.854 billion years (Ga) ago must be consistent with several lines of seemingly contradictory evidence. First, strong palaeomagnetic intensity measurements (for example, 69 ± 16 μT) have been recovered from returned Apollo samples that formed during this period[1]. Second, lunar swirls—high-albedo surface features associated with high magnetic-field strengths[2]—are also consistent with the existence of a high-intensity lunar dynamo at times between 3.3 and 3.9 Ga (ref. 3). Third and conversely, over the same period, weak and null palaeointensity measurements have been recovered from Apollo samples[4,5], and weakly magnetized (<1 nT) craters have been reported[6–8]. Finally, although strong crustal magnetic anomalies with an age of 3.7–3.9 Ga are observed at the antipodes of large impact basins, they are shown to be consistent with a weak dynamo field (~1 μT) amplified by impact-generated plasma fields[9]. Although variable preservation and detection biases complicate interpretation (Supplementary Information section 1), these observations point towards a generally weak lunar magnetic field with intermittent high-intensity interludes. We therefore refer to this period as the Intermittent High Intensity Epoch (IHIE).

The observed high palaeointensity measurements during the IHIE (Fig. 1) are particularly difficult to explain given the small size of the lunar core and the limited energy available to drive a dynamo[10,11]. Convective dynamos can sustain only a weak surface magnetic field (<11 μT) for the duration of the IHIE[11]. Several other mechanisms have been proposed to explain a sustained magnetic field that gradually decreases in strength over time by considering gravitational stirring of the lunar core[12,13] or invoking a basal magma ocean coupled with core solidification[14,15]. However, these models cannot explain surface fields exceeding 30 μT and were not designed to explore the apparent intermittency observed throughout the IHIE suggested by more recent palaeointensity measurements[4,5].

A notable feature of the IHIE is the eruption of high-Ti mare basalts, which contain >6 wt% $TiO_2$ (ref. 16). These basalts were recovered by the Apollo 11 and 17 missions. High-Ti basalts with ages spanning 1.0–3.9 Ga have also been detected from remote-sensing data, although they make up a small proportion of total mare volcanism[17,18] (Fig. 1 and Supplementary Information section 2). In contrast to low-Ti basalts, high-Ti magmas cannot be formed by equilibrium partial melting of the lunar mantle, but require a mixed source containing both

Department of Earth Sciences, University of Oxford, Oxford, UK. ✉e-mail: claire.nichols@earth.ox.ac.uk

https://doi.org/10.1038/s41561-026-01929-y

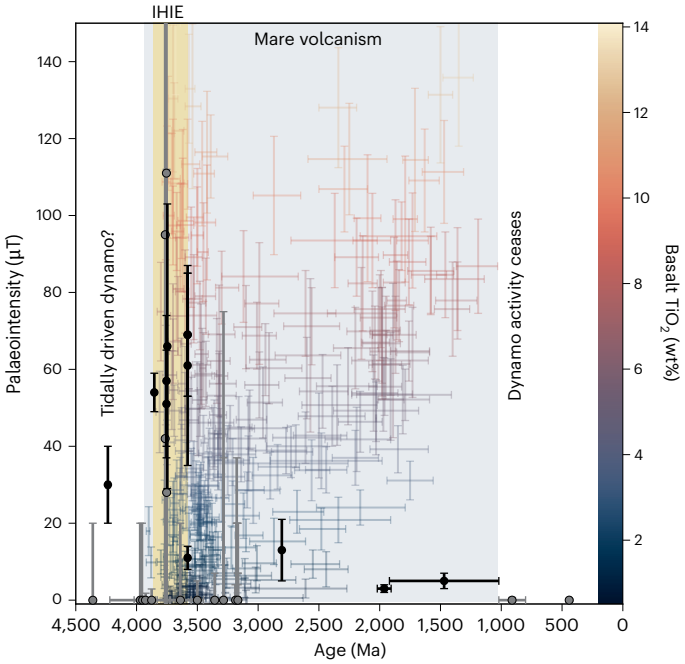


**Fig. 1 | The age and composition of lunar mare volcanism compared with the palaeointensity record.** Non-null palaeointensities (black circles represent mean values) and palaeointensities within an error of zero (grey circles represent mean values) with 1$\sigma$ palaeointensity uncertainty reported from literature (vertical error bars) and 2$\sigma$ age uncertainty from U–Pb dating (horizontal error bars) for returned samples (Supplementary Table 1) are compared with the age and composition of lunar mare basalts based on crater counting and remote spectral data (coloured error bars; 1$\sigma$ uncertainty reported from literature[17,18]). Light blue box represents the total duration of mare volcanism; the yellow box represents the duration of the IHIE used in this study. All but one of the non-null palaeointensities coincides with the duration of mare volcanism, and this early palaeointensity may be explained by tidal heating[48] (Supplementary Information section 2).

mantle and ilmenite-bearing cumulate material[19,20]. Several studies have proposed that the high-Ti basalts originate by partial melting of ilmenite-bearing cumulates at the core–mantle boundary (CMB) after mantle overturn[21–24]. However, others argue that the source melts must originate in the upper or middle mantle and suggest that high-Ti melts become increasingly dense with depth, reducing the likelihood of their return to the surface[25–28]. Notwithstanding the lack of consensus concerning the source depth of high-Ti basalts, at least some partially molten ilmenite-bearing cumulates are thought to reside at the CMB. Indeed, their presence is required to explain lowermost mantle seismic signatures[10,27].

The presence of ilmenite-bearing cumulate material at the CMB has been proposed to have triggered lunar dynamo activity[29,30]. It is possible to generate a dynamo, or at least enhance existing activity, by temporarily elevating the heat flux across the CMB. Elevated heat flow can be achieved in one of two ways. First, the latent heat of melting ilmenite-bearing cumulates can drive a sharp increase in thermal flux across the CMB, initiating a short-lived, high-intensity dynamo[29]. Second, as the cumulates melt, they may become buoyant and rise away from the CMB[30]. Removal of this hotter, radiogenically heated material could also temporarily elevate the CMB heat flux. However, in either case, strong magnetic fields can be sustained for only a fraction of the IHIE because of the limited core energy budget[11]. It is therefore challenging to explain why such a high proportion of Apollo samples (7 out of 13) with ages within the IHIE record a magnetic field exceeding 20 μT.

If melting of ilmenite-bearing cumulates drives both dynamo activity and the formation of high-Ti basalts, then a link may exist between palaeointensity and basalt composition. To test this possibility, we examine the relationship between palaeointensity and the Ti content of Apollo samples. We assess whether compositional controls are required to explain the palaeomagnetic record and consider the implications for the source depth of high-Ti basalts and lunar mantle overturn.

## A link between high-Ti basalts and strong magnetic fields

We find that all strong palaeointensities are exclusively recorded by high-Ti basalts while weak palaeointensities, within uncertainty of zero, are recorded by a range of lunar lithologies (Supplementary Figs. 1 and 2 and Supplementary Table 1). Within the IHIE, all palaeointensity measurements have been made on lunar basalts. Throughout mare volcanism, the low-Ti basalts return a significantly lower weighted mean palaeointensity, $B_{anc} = 2 \pm 7$ μT, than the high-Ti basalts, $B_{anc} = 27 \pm 23$ μT (Fig. 2a and Supplementary Tables 2 and 3). Despite the small number of measured samples and their large associated uncertainties, we find that the weighted mean palaeointensities for the low- and high-Ti basalts are statistically distinct (Mann–Whitney $U = 0.0$, $P = 1.4 \times 10^{-4}$). This result suggests that high- and low-Ti basalts are unlikely to have been randomly drawn from the same background palaeointensity distribution.

Next, we compare the recovered palaeointensity measurements with other geochemical and rock magnetic properties of lunar basalts. We find the strongest statistically significant positive correlation is between palaeointensity and $TiO_2$ wt% ($r = 0.72$, $P = 1.7 \times 10^{-4}$; Fig. 2). There are also significant correlations between age and $TiO_2$ wt% ($r = 0.71$) and between age and palaeointensity ($r = 0.54$). Other correlations between geochemical and magnetic hysteresis parameters[31] are markedly less strong and are unlikely to be significant when analytical uncertainties are included (Fig. 2b and Supplementary Figs. 3–6). We find no strong relationship between $TiO_2$ wt% and magnetic hysteresis parameters, $M_{rs}/M_s$ and $H_{cr}/H_c$, suggesting that potential confounding controls, such as a systematic difference in magnetic carriers that would influence palaeomagnetic fidelity, are unlikely to account for their covariance. Similarly, the lack of correlation between palaeointensity and the other chemical components, $K_2O$ wt%, Sm/Nd and Mg#, suggest processes such as fractional crystallization do not play a role. These correlations, or the lack thereof, therefore suggest an external confounding variable is driving the observed relationship between palaeointensity and the Ti content of lunar basalts.

Our results can be explained in two ways. In scenario 1, the lunar dynamo is intermittently strong during the IHIE but, on average, operates at high intensity for a greater proportion of time before it gradually declines after the IHIE, as proposed by previous studies[31,32]. The apparent correlation with high-Ti basalts is incidental. In scenario 2, the dynamo need not be active for a large proportion of the IHIE. Instead, episodes of high magnetic-field intensity are causally linked to the melting of ilmenite-bearing cumulates at the CMB and the generation of high-Ti basalts[30,33]. Under this scenario, greater sampling of high-Ti basalts during the IHIE would bias the record towards an apparently more persistently intense field.

## A dynamo driven by melting of ilmenite-bearing cumulates

Next we investigate whether either of the proposed dynamo mechanisms that involve ilmenite-bearing cumulates[29,30] can recreate the observed palaeointensity record without invoking a link between high-Ti basalts and elevated dynamo activity (scenario 1). Each dynamo mechanism must satisfy four criteria dictated by the modern palaeomagnetic record of the lunar dynamo (Methods). First, the dynamo must be intermittently active for at least 274 Ma. Second, the dynamo must be able to exceed a surface magnetic-field intensity of 53 μT. Third, the duration of each discrete period of dynamo activity must last at least 100 days ($2.7 \times 10^{-5}$ ka). Fourth, the dynamo must be active for at least 1% of the IHIE.

https://doi.org/10.1038/s41561-026-01929-y

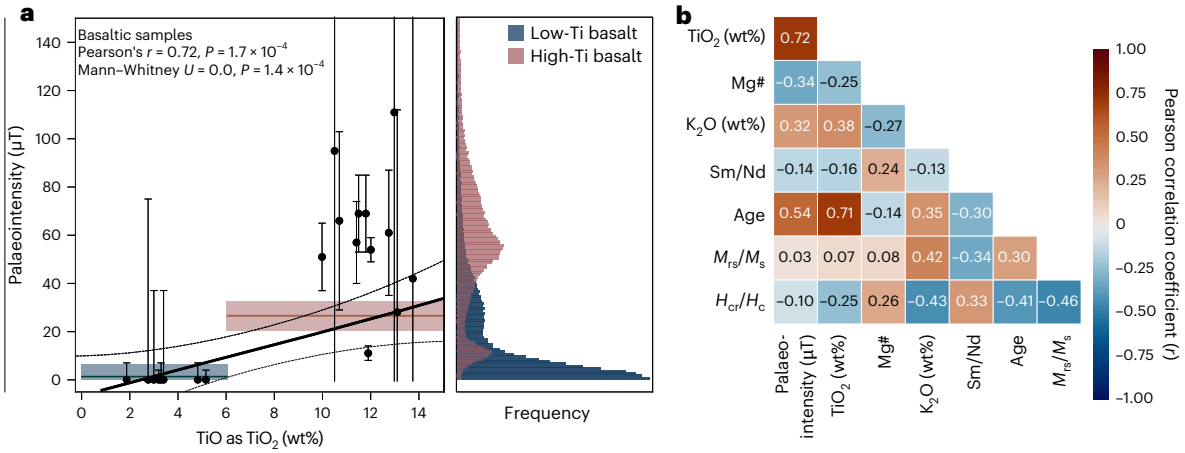


**Fig. 2 | The relationship between palaeointensity and $TiO_2$ wt% in lunar Apollo samples. a**, Palaeointensity as a function of $TiO_2$ wt% from existing data (Supplementary Table 1). Black circles represent mean palaeointensity and maximum reported $TiO_2$ wt% in the literature (Supplementary Table 1). Error bars represent 1$\sigma$ uncertainty. Palaeointensity measurements reported without uncertainty have been excluded. Bold black line represents two-sided weighted linear regression and 95% confidence interval (black dashed line). Blue horizontal line represents weighted mean palaeointensity value for low-Ti (<6 wt% $TiO_2$) basalts. Red horizontal line represents weighted mean palaeointensity value for high-Ti (>6 wt% $TiO_2$) basalts. Shaded regions represent precision on mean value for each group. Histograms show the distribution of palaeointensity measurements for low- and high-Ti basalts in blue and red, respectively. **b**, A correlation matrix for Pearson's correlation coefficient, $r$, for palaeointensity, $TiO_2$ wt%, Mg#, $K_2O$ wt%, Sm/Nd ratio, age and magnetic hysteresis parameters $M_{rs}/M_s$ and $H_{cr}/H_c$ for all lunar basalts for which palaeointensity and/or magnetic hysteresis measurements exist. The only strong correlations ($r > 0.5$) are between $TiO_2$ wt%, age and palaeointensity.

Our first model considers the mechanism of dynamo generation proposed by Evans and Tikoo[29], where ilmenite-bearing cumulates sink to the CMB during protracted mantle overturn and melt atop the core. As expected, our simulations are capable of yielding a stochastic, intense dynamo that is intermittently active for hundreds of millions of years for a wide range of parameter combinations (Methods), broadly reflecting the existing palaeomagnetic record throughout the IHIE. Importantly, all of the simulations can sustain a continuous dynamo for >100 days. Furthermore, many simulations generate an intermittent dynamo for > 274 Ma with an intensity exceeding 53 μT. Crucially however, no simulation simultaneously satisfies these criteria while also driving a dynamo for >1% of the IHIE (Fig. 3). These criteria cannot be met simultaneously because there is a direct trade-off between producing sufficiently high field intensities—requiring very short melting events—and the cumulative duration of the melting events being long enough to last >1% of the duration of the IHIE (Supplementary Information section 3). In the optimal case, descent of Ti-rich diapirs to the CMB is capable of sustaining a dynamo for only <0.2% of the IHIE (Fig. 3), indicating either a predominantly inactive or a predominantly weak dynamo. This dynamo mechanism therefore fails to reproduce the observed palaeomagnetic record for scenario 1 because the field is not pervasively operating at high intensity. However, in scenario 2 there is a bias towards capturing these rare, high-intensity events. The existing palaeomagnetic record during the IHIE is exclusively preserved in high-Ti basalts; thus, the chances of capturing high-intensity events is far more likely, reflecting the observed palaeomagnetic record.

Next we consider the feasibility of the dynamo mechanism proposed by Stegman and coauthors[30], where ilmenite-bearing cumulates are radiogenically heated and melt at the CMB after mantle overturn has ended (Methods). The constraints for this second model are less restrictive than for the first since melting of ilmenite-bearing cumulates post-dates their arrival at the CMB. Therefore, we assume that the entire volume observed at the CMB today can melt in a single event of finite duration. We also assume cumulates can melt repeatedly throughout the IHIE, and therefore the dynamo can be intermittently active for >274 Ma, fulfilling one of our observational criteria. The remaining three observational criteria—the intensity of the surface magnetic field, the duration of individual high-intensity dynamo events and the cumulative proportion of high-intensity dynamo activity—are governed by the volume and duration of melting at the CMB. To generate the observed high-intensity surface magnetic fields, we find that the entire ilmenite-bearing cumulate layer would need to melt in <4.7 ka (Methods and Fig. 4). Such a rapid melting rate implies that roughly 600 discrete events would be required to sustain a high-intensity dynamo for just 1% of the IHIE.

While the model proposed by Stegman and coauthors[30] can potentially fulfil the observational criteria, this is only for the case where the ilmenite-bearing cumulate layer repeatedly melts entirely. Petrological evidence indicates that the high-Ti basalts are generated by a melt fraction between 20 and 40% (ref. 20), suggesting that, in reality, periods of intense dynamo activity are much shorter than 4.7 ka. Therefore, the very short-lived high-intensity dynamo events will result in a pervasively weak magnetic field during the IHIE, at odds with scenario 1. We therefore argue that under either mechanism of dynamo generation, it is necessary that the melting of ilmenite-bearing cumulates can simultaneously generate high-Ti basalts and strong magnetic fields, a conclusion that supports scenario 2. Again, such a conclusion potentially points towards a bias in the lunar palaeomagnetic record, whereby rare, high-intensity magnetic fields are repeatedly sampled by the coincident eruption of high-Ti basalts.

## Lunar dynamics during the IHIE

Our modelling results suggest that there is a genuine association between high-intensity dynamo activity and the eruption of high-Ti basalts, indicating that melting of ilmenite-bearing cumulates sufficiently elevates the CMB heat flux to drive a short-lived, intense dynamo (Fig. 5). We favour a dynamo driven by radiogenic heating of ilmenite-bearing cumulates at the CMB after mantle overturn[30] since a dynamo driven by protracted mantle overturn[29] extending into the IHIE requires mantle overturn to last an order of magnitude longer than predicted by simulations of thermo-chemical mantle convection[34]. However, the ability of either mechanism to generate a dynamo, and the detail of its behaviour, requires further validation using magnetohydrodynamic simulations. In addition, to be dynamically feasible requires the union of three processes and their timescales of operation. First, the ilmenite-bearing cumulates must melt sufficiently quickly to

https://doi.org/10.1038/s41561-026-01929-y

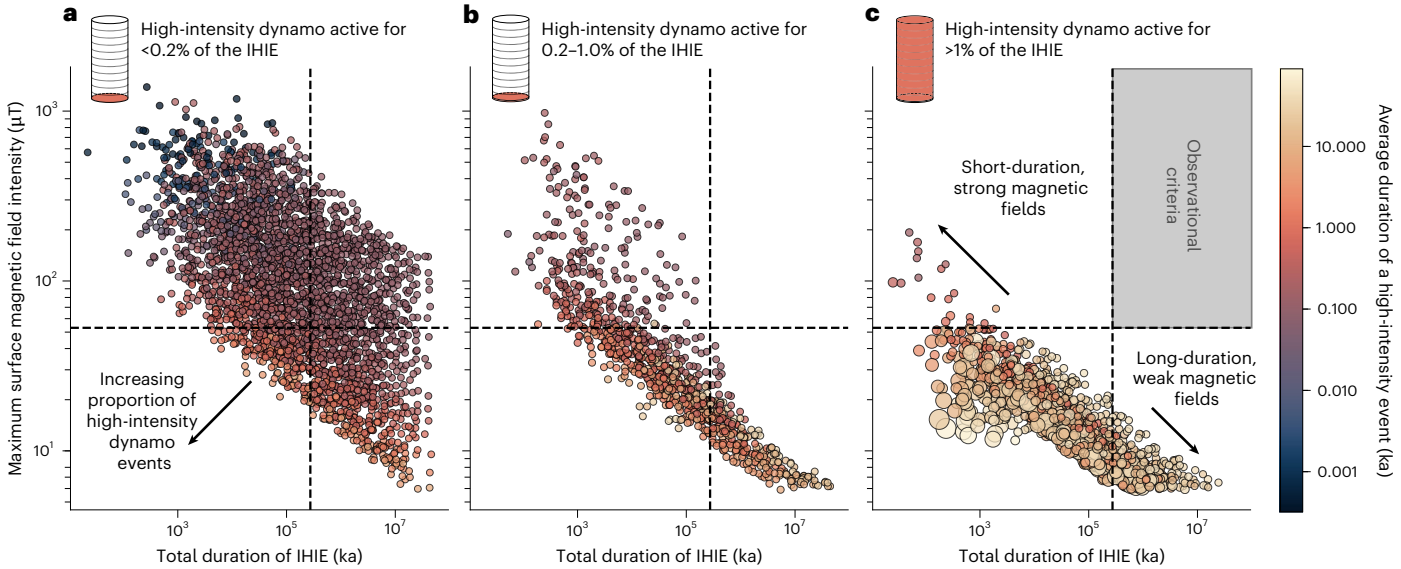


**Fig. 3 | Model results for a dynamo generated by protracted mantle overturn.** Scatter plots showing results for the four observational criteria for each model run. The maximum magnetic-field intensity (*y* axis) must exceed 53 μT (horizontal dashed line). The total duration of the IHIE (*x* axis) must exceed 274 Ma (vertical dashed line). The average duration of an event (colour bar) must exceed 100 days, and this criterion is passed in all cases. The cumulative percentage of time over which a high-intensity dynamo is generated (circle size) must exceed 1% of the IHIE. **a**, All model outputs where the cumulative percentage of time in which a high-intensity dynamo is active is < 0.2%, which allows sufficiently strong magnetic fields to be generated for the observed duration of the IHIE thereby fulfilling three of the four observational criteria. **b**, Model outputs where the high-intensity dynamo is active for between 0.2 and 1.0% of the IHIE. In this case, strong fields can be generated, or the IHIE can last for the required time, but these two criteria cannot be fulfilled simultaneously. **c**, Model outputs in which the high-intensity dynamo is active for more than 1% of the IHIE, highlighting the fact that all four observational criteria are never simultaneously met (grey region).

generate the observed surface magnetic-field intensities. Second, melts must ascend from the CMB to the surface and erupt as high-Ti basalts while the high-intensity dynamo is active. Finally, high-Ti basalts must cool through their Curie temperature and acquire a palaeomagnetic remanence before high-intensity dynamo activity ceases.

We have shown that ilmenite-bearing cumulate melting events must last <4.7 ka to generate the observed palaeointensities (Fig. 4), and therefore high-Ti basalts must also erupt within this time. This eruptive timescale is similar to those for flood basalts on Earth, which typically have eruption durations of <2 ka between hiatuses lasting from $1 \times 10^{-3}$ to 10 ka (ref. 35). A recent study on magnesium isotopic signatures in high-Ti basalts suggests they interact with the ambient mantle for just 1–30 days (ref. 19), implying that ascent is much quicker than the required melting time. Rapid ascent of high-Ti basalts could be facilitated by the presence of high-permeability dunite channels, which have been shown to form when melts rise through the ambient harzburgitic mantle, allowing the fast rise of subsequent melts[36]. Once at the surface, cooling below the Curie temperature takes less than 100 days (refs. 37,38). Thus, while high-intensity dynamo activity lasts on the order of $10^3$ years, the subsequent ascent, eruption and palaeomagnetic remanence acquisition of high-Ti basalts probably takes only months. Taken together, these timescales suggest it is plausible that melting of ilmenite-bearing cumulates at the CMB can simultaneously generate a high-intensity magnetic field while high-Ti basalts are emplaced on the lunar surface, thus recording this transient, intense magnetic field.

The link between high-Ti basaltic eruptions and an elevated CMB heat flux suggests that ilmenite-bearing cumulate melts are buoyant at all depths within the lunar mantle. This negates the requirement for high-Ti basalts to have a source region in the mid-mantle, as suggested in several studies[20,25,26,28]. An origin for Ti-rich melts at the CMB is supported by recent high-pressure and temperature experiments[39] as well as molecular dynamical simulations[40]. Recent work has also suggested that the buoyancy of Ti-rich melts is further enhanced by Fe–Mg exchange with the ambient mantle[19,41]. A CMB origin for ilmenite-bearing cumulates is also consistent with the lack of evidence for this material in the mid-mantle[42].

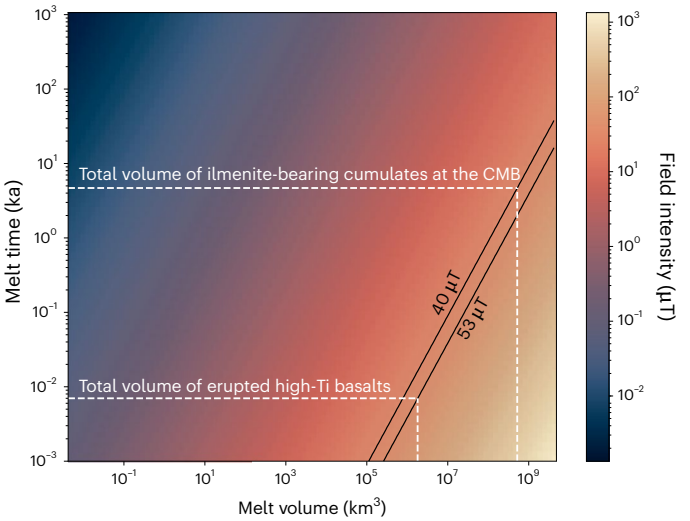


**Fig. 4 | Model results for melting of ilmenite-bearing cumulates at the CMB.** Surface magnetic field (colour bar) as a function of melting time and melt volume of ilmenite-bearing cumulates. Black contours represent surface magnetic fields of 40 and 53 μT, the minimum required magnetic-field intensity required to explain the palaeointensities recovered by high-Ti basalts in each eruptive period. White vertical dashed lines represent upper and lower limits on the volume of ilmenite-bearing cumulates that melt. White horizontal dashed lines represent the upper limit on the melting times for the upper and lower melt volume estimates to generate the required surface magnetic fields.

The distribution of ilmenite-bearing cumulates within the lunar mantle has further implications for the nature of mantle overturn. Ilmenite-bearing cumulates originated at the top of the lunar mantle

https://doi.org/10.1038/s41561-026-01929-y

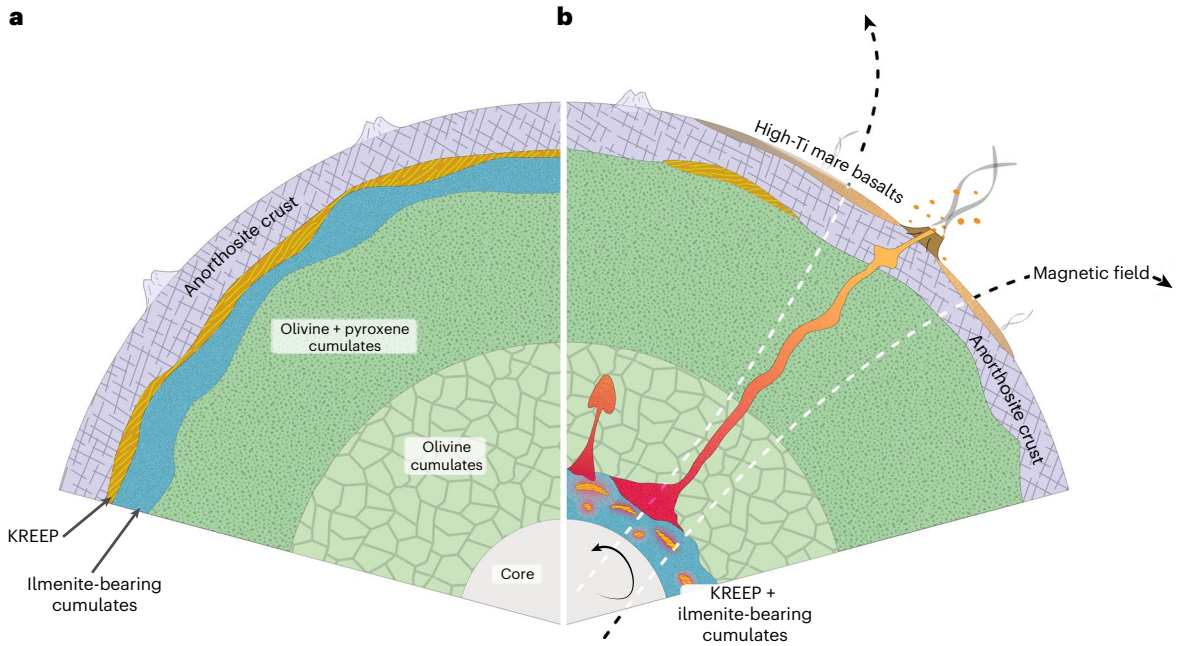


**Fig. 5 | Radiogenic heating of ilmenite-bearing cumulates generates a high-intensity dynamo field and the eruption of high-Ti basalts. a**, The structure of the Moon at the end of magma ocean solidification. Dense, ilmenite-bearing cumulates and KREEP material crystallize at the top of the lunar mantle. The cumulates are gravitationally unstable and subsequently sink to the CMB, entraining some KREEP material. **b**, The lunar regime during the IHIE. Radiogenic heat produced by KREEP material sufficiently warms the base of the mantle to initiate mantle convection and the melting of ilmenite-bearing cumulates. Melting of these cumulates at the CMB temporarily elevates the heat flux out of the core, driving a short-lived, high-intensity dynamo. Simultaneously, high-Ti basalts erupt on the surface, capturing the rare occurrence of a strong lunar magnetic field.

at the end of magma ocean solidification[43]. However, these cumulates are denser than the ambient mantle and therefore were gravitationally unstable, leading to their subsequent transportation into the deep lunar interior (Fig. 5). Several different possibilities have been considered for this mantle overturn event, which we briefly discuss.

Several studies suggest that mantle overturn occurs on small length scales, with numerous diapirs of ilmenite-rich cumulate material sinking to the CMB. This process is generally found to occur within a few hundred million years, pre-dating the IHIE[34,44,45]. Studies that explore short length-scale overturn indicate that partial overturn is feasible, such that some ilmenite-bearing cumulates may founder at mid-mantle depths rather than at the CMB. Foundering of Ti-rich material in the mid-mantle typically occurs at higher mantle viscosities[45] and aligns well with previous petrological studies[20,25,26,28]. However, these models also result in partially molten ilmenite-bearing cumulate material at the CMB that is negatively buoyant, creating a thermal blanket that inhibits a lunar dynamo[27,44]. These models therefore predict the eruption of high-Ti basalts from a mid-mantle source in the absence of a dynamo, contrary to the consistently high palaeointensity measurements recovered exclusively by these lavas (Fig. 2).

Other studies predict rapid (within the first 100 Ma after lunar magma ocean solidification), wholescale overturn of the gravitationally unstable ilmenite-bearing cumulate layer to the CMB[24,30,33,46]. Once at the CMB, radiogenic heating from entrained material enriched in potassium, rare-earth elements and phosphorus (KREEP) leads to the thermal expansion of the ilmenite-bearing cumulates. This heating also triggers the onset of mantle convection ~500 Ma after magma ocean solidification, allowing hot, buoyant Ti-rich melts to become re-entrained into the overlying mantle[47]. This entrainment coincides with the onset of the IHIE ~3.85 Ga. The melting and rising of cumulates can drive a dynamo[30] and may also trigger the eruption of high-Ti basalts[24,30,33,47]. These studies therefore predict that high-Ti basalts should erupt in the presence of a magnetic field, consistent with our observational findings.

Our results indicate that high-Ti basaltic eruptions and intense dynamo activity occurred during the melting and re-entrainment of ilmenite-bearing cumulates at the CMB several hundred million years after mantle overturn[24,30,33]. Both phenomena are short-lived, collectively operating on a timescale of thousands of years during the IHIE, but are overrepresented in Apollo samples due to landing sites near high-Ti mare basalt terranes. This sampling bias helps reconcile the apparent mismatch between the lunar energy budget and the strong palaeointensity values from high-Ti basalts[11].

## Online content

Any methods, additional references, Nature Portfolio reporting summaries, source data, extended data, supplementary information, acknowledgements, peer review information; details of author contributions and competing interests; and statements of data and code availability are available at https://doi.org/10.1038/s41561-026-01929-y.

## References

1. Suavet, C. et al. Persistence and origin of the lunar core dynamo. *Proc. Natl Acad. Sci. USA* **110**, 8453–8458 (2013).
2. Kramer, G. Y. et al. Characterization of lunar swirls at Mare Ingenii: a model for space weathering at magnetic anomalies. *J. Geophys. Res. Planets* **116**, E04008 (2011).
3. Weiss, B.P. & Tikoo, S. The lunar dynamo. *Science* **346**, 1246753 (2014).
4. Tarduno, J. A. et al. Absence of a long-lived lunar paleomagnetosphere. *Sci. Adv.* **7**, eabi7647 (2021).
5. Zhou, et al. A lunar core dynamo limited to the Moon's first ~140 million years. *Commun. Earth Environ.* **5**, 456 (2024).
6. Hood, L. L. & Spudis, P. D. Magnetic anomalies in the Imbrium and Schrödinger impact basins: orbital evidence for persistence of the lunar core dynamo into the Imbrian epoch. *J. Geophys. Res. Planets* **121**, 2268–2281 (2016).

7. Wieczorek, M. A., Weiss, B. P. & Stewart, S. T. An impactor origin for lunar magnetic anomalies. *Science* **335**, 1212–1215 (2012).
8. Wieczorek, M. et al. Lunar Magnetism. *Rev. Mineral. Geochem.* **89**, 207–242 (2023).
9. Narrett, I. S. et al. Impact plasma amplification of the ancient lunar dynamo. *Sci. Adv.* **11**, eadr7401 (2025).
10. Weber, R. C., Lin, P.-Y. Y., Garnero, E. J. E. J., Williams, Q. C. & Lognonné, P. Seismic detection of the lunar core. *Science* **331**, 309–312 (2011).
11. Evans, A. J., Tikoo, S. M. & Andrews-Hanna, J. C. The case against an early lunar dynamo powered by core convection. *Geophys. Res. Lett.* **45**, 98–107 (2018).
12. Dwyer, C. A., Stevenson, D. J. & Nimmo, F. A long-lived lunar dynamo driven by continuous mechanical stirring. *Nature* **479**, 212–214 (2011).
13. Stys, C. & Dumberry, M. A past lunar dynamo thermally driven by the precession of its inner core. *J. Geophys. Res.* **125**, e2020JE006396 (2020).
14. Scheinberg, A. L., Soderlund, K. M. & Elkins-Tanton, L. T. A basal magma ocean dynamo to explain the early lunar magnetic field. *Earth Planet. Sci. Lett.* **492**, 144–151 (2018).
15. Hamid, S. S., O'Rourke, J. G. & Soderlund, K. M. A long-lived lunar magnetic field powered by convection in the core and a basal magma ocean. *Planet. Sci. J.* **4**, 18 (2023).
16. Neal, C. & Taylor, L. Petrogenesis of mare basalts: a record of lunar volcanism. *Geochim. Cosmochim. Acta* **56**, 2177–2211 (1992).
17. Qian, Y. et al. Mineralogy and chronology of the young mare volcanism in the Procellarum–KREEP–Terrane. *Nat. Astron.* **7**, 287–297 (2023).
18. Kato, S. et al. Magma source transition of lunar mare volcanism at 2.3 Ga. *Meteorit. Planet. Sci.* **52**, 1899–1915 (2017).
19. Klaver, M. et al. Titanium-rich basaltic melts on the Moon modulated by reactive flow processes. *Nat. Geosci.* **17**, 118–123 (2024).
20. Haupt, C. P., Renggli, C. J., Rohrbach, A., Berndt, J. & Klemme, S. Experimental constraints on the origin of the lunar high-Ti basalts. *J. Geophys. Res. Planets* **129**, e2023JE008239 (2024).
21. Su, B. et al. Fusible mantle cumulates trigger young mare volcanism on the cooling Moon. *Sci. Adv.* **8**, eabn2103 (2022).
22. Kesson, S. E. & Ringwood, A. E. Mare basalt petrogenesis in a dynamic moon. *Earth Planet. Sci. Lett.* **30**, 155–163 (1976).
23. Hess, P. C. & Parmentier, E. M. A model for the thermal and chemical evolution of the Moon's interior: implications for the onset of mare volcanism. *Earth Planet. Sci. Lett.* **134**, 501–514 (1995).
24. Zhong, S., Parmentier, E. M. & Zuber, M. T. A dynamic origin for the global asymmetry of lunar mare basalts. *Earth Planet. Sci. Lett.* **177**, 131–140 (2000).
25. Elkins Tanton, L. T., Van Orman, J. A., Hager, B. H. & Grove, T. L. Re-examination of the lunar magma ocean cumulate overturn hypothesis: Melting or mixing is required. *Earth Planet. Sci. Lett.* **196**, 239–249 (2002).
26. Singletary, S. & Grove, T. Origin of lunar high-titanium ultramafic glasses: a hybridized source?. *Earth Planet. Sci. Lett.* **268**, 182–189 (2008).
27. Xu, M., Jing, Z., Van Orman, J. A., Yu, T. & Wang, Y. Experimental evidence supporting an overturned iron-titanium-rich melt layer in the deep lunar interior. *Geophys. Res. Lett.* **49**, e2022GL099066 (2022).
28. Gao, S., Lin, Y. & van Westrenen, W. Experimental evidence for a shallow cumulate remelting origin of lunar high-titanium mare basalts. *Commun. Earth Environ.* **6**, 59 (2025).
29. Evans, A. J. & Tikoo, S. M. An episodic high-intensity lunar core dynamo. *Nat. Astron.* **6**, 325–330 (2022).
30. Stegman, D. R., Jellinek, A. M., Zatman, S. A., Baumgardner, J. R. & Richards, M. A. An early lunar core dynamo driven by thermochemical mantle convection. *Nature* **421**, 143–146 (2003).
31. Strauss, B. E., Tikoo, S. M., Gross, J., Setera, J. B. & Turrin, B. Constraining the decline of the lunar dynamo field at ≈ 3.1 Ga through paleomagnetic analyses of Apollo 12 mare basalts. *J. Geophys. Res.* **126**, e2020JE006715 (2021).
32. Tikoo, S. M. et al. Decline of the lunar core dynamo. *Earth Planet. Sci. Lett.* **404**, 89–97 (2014).
33. Zhang, N., Parmentier, E. M. & Liang, Y. A 3-D numerical study of the thermal evolution of the Moon after cumulate mantle overturn: the importance of rheology and core solidification. *J. Geophys. Res. Planets* **118**, 1789–1804 (2013).
34. Maurice, M., Tosi, N. & Hüttig, C. Small-scale overturn of high-Ti cumulates promoted by the long lifetime of the lunar magma ocean. *J. Geophys. Res. Planets* **129**, e2023JE008060 (2024).
35. Self, S., Schmidt, A. & Mather, T. A. Emplacment characteristics, time scales, and volcanic gas release rates of continental flood basalt eruptions on Earth. In *Volcanism, Impacts, and Mass Extinctions: Causes and Effects: Geological Society of America Special Paper* 505 (eds Keller, G. & Kerr, A.C.) 319–337 (2014).
36. Beck, A. R., Morgan, Z. T., Liang, Y. & Hess, P. C. Dunite channels as viable pathways for mare basalt transport in the deep lunar mantle. *Geophys. Res. Lett.* **33**, L01202 (2006).
37. Grove, T. L. & Walker, D. Cooling histories of Apollo 15 quartz normative basalts. In *Proc. 8th Lunar Sci. Conf.* 1501–1520 (1977).
38. Donaldson, C. H., Usselman, T. M., Williams, R. J. & Lofgren, G. E. Experimental modeling of the cooling history of Apollo 12 olivine basalts. In *Proc. 6th Lunar Sci. Conf.* 843–869 (1975).
39. Vander Kaaden, K. E., Agee, C. B. & McCubbin, F. M. Density and compressibility of the molten lunar picritic glasses: implications for the roles of Ti and Fe in the structures of silicate melts. *Geochim. Cosmochim. Acta* **149**, 1–20 (2015).
40. Van Kan Parker, M. et al. Neutral buoyancy of titanium-rich melts in the deep lunar interior. *Nat. Geosci.* **5**, 186–189 (2012).
41. Mallik, A., Ejaz, T., Shcheka, S. & Garapic, G. A petrologic study on the effect of mantle overturn: implications for evolution of the lunar interior. *Geochim. Cosmochim. Acta* **250**, 238–250 (2019).
42. Grimm, R. E. Lunar mantle structure and composition inferred from Apollo 12 – Explorer 35 electromagnetic sounding. *Icarus* **407**, 115775 (2024).
43. Elkins-Tanton, L. T., Burgess, S. & Yin, Q. Z. The lunar magma ocean: reconciling the solidification process with lunar petrology and geochronology. *Earth Planet. Sci. Lett.* **304**, 326–336 (2011).
44. Zhao, Y., de Vries, J., van den Berg, A. P., Jacobs, M. H. G. & van Westrenen, W. The participation of ilmenite-bearing cumulates in lunar mantle overturn. *Earth Planet. Sci. Lett.* **511**, 1–11 (2019).
45. Yu, S. et al. Overturn of ilmenite-bearing cumulates in a rheologically weak lunar mantle. *J. Geophys. Res. Planets* **124**, 418–436 (2019).
46. Parmentier, E. M., Zhong, S. & Zuber, M. T. Gravitational differentiation due to initial chemical stratification: origin of lunar asymmetry by the creep of dense KREEP?. *Earth Planet. Sci. Lett.* **201**, 473–480 (2002).
47. Laneuville, M., Wieczorek, M. A., Breuer, D. & Tosi, N. Asymmetric thermal evolution of the Moon. *J. Geophys. Res. Planets* **118**, 1435–1452 (2013.
48. Nimmo, F., Kleine, T. & Morbidelli, A. Tidally driven remelting around 4.35 billion years ago indicates the Moon is old. *Nature* **636**, 598–602 (2024).

**Publisher's note** Springer Nature remains neutral with regard to jurisdictional claims in published maps and institutional affiliations.

**Open Access** This article is licensed under a Creative Commons Attribution 4.0 International License, which permits use, sharing, adaptation, distribution and reproduction in any medium or format, as long as you give appropriate credit to the original author(s) and the source, provide a link to the Creative Commons licence, and indicate if changes were made. The images or other third party material in this article are included in the article's Creative Commons licence, unless indicated otherwise in a credit line to the material. If material is not included in the article's Creative Commons licence and your intended use is not permitted by statutory regulation or exceeds the permitted use, you will need to obtain permission directly from the copyright holder. To view a copy of this licence, visit http://creativecommons.org/licenses/by/4.0/.

© The Author(s) 2026

# Methods

## Composition, magnetic hysteresis and palaeointensity statistical analysis

Palaeointensity measurements from the IHIE are divided into three categories: palaeointensities whose 1$\sigma$ uncertainties are not within error of zero[1,49–51], palaeointensities that are within uncertainty of zero[4,5,52], and palaeointensities that exceed 20 μT by at least 1$\sigma$ (refs. 1,49,51; Supplementary Fig. 7).

We examine the link between $TiO_2$ wt% and the recovered palaeointensity for all basaltic samples that have undergone palaeomagnetic analysis. For each sample, we take the highest measured $TiO_2$ wt% from the literature[53] and compare this with the recovered palaeointensity and associated uncertainties. We do not include samples where a stable remanence could not be recovered[52,54]. To investigate the statistical relationship between composition and palaeointensity, we carry out several statistical tests.

To quantify the association between high-Ti basalts and high palaeointensity measurements, we split the palaeointensity measurements recovered from low- and high-Ti basalts into two populations for samples where a palaeointensity is reported with a calculated 1$\sigma$ uncertainty. We calculate a weighted mean palaeointensity value for each group. This is done by scaling the contribution of each sample to the mean population by its reported uncertainty such that better-constrained estimates contribute proportionally more to the mean. We divide the data into two populations: low-Ti basalts, where $TiO_2 < 6$ wt%, and high-Ti basalts, where $TiO_2 > 6$ wt%. For each population, we calculate the weighted mean

$$\bar{x} = \frac{\sum_{i=0}^{i=n} w_i x_i}{\sum_{i=0}^{i=n} w_i} \tag{1}$$

where $w_i = \frac{1}{\sigma_i^2}$ is the weighted variance and is given by

$$\bar{\sigma} = \sqrt{\left( \frac{\sum_{i=0}^{i=n} w_i (x_i - \bar{x})^2}{\frac{n-1}{n} \sum_{i=0}^{i=n} w_i} \right)} \tag{2}$$

and $\frac{1}{\sum_{i=0}^{i=n} w_i}$ is the precision. We then compare these populations by carrying out a Mann–Whitney $U$ test using the Python SciPy.stats package. We take the weighted mean, variance and number of samples from the low- and high-Ti groups. In the case of upper limits on palaeointensity, we take the mean to be zero and one standard deviation to be the upper limit. Next, we draw 10,000 samples from each distribution. We then rank these truncated, normal distributions (palaeointensity values cannot be negative) to determine whether the two distributions are different with statistical significance. These populations are used to create histograms to compare the distribution of palaeointensity values for the low- and high-Ti basalts, respectively (Supplementary Tables 2 and 3). A similar approach is also used to compare magnetic hysteresis properties between high- and low-Ti basalts (Supplementary Fig. 3).

To further quantify the link between palaeointensity and petrologic composition, we evaluate correlations between compositional ($TiO_2$ wt%, $K_2O$ wt%, Mg# and Sm/Nd), palaeointensity and magnetic hysteresis parameters ($M_{rs}/M_s$ and $H_{cr}/H_c$) for all lunar basalts for which palaeointensity and/or hysteresis measurements exist (Supplementary Table 4). We perform a weighted linear regression for all palaeointensities plotted against each composition using the statsmodels package in Python. We use this to find the best-fit line through the data and associated 95% confidence interval. Next we use the Pandas library DataFrame.corr() to calculate pairwise Pearson correlation coefficients ($r$ and $P$ values) between all parameters.

## Reconciling dynamo models with the palaeomagnetic record

Our models must meet four criteria set by the lunar palaeomagnetic record. First, the dynamo must be intermittently active for at least 274 Ma, a constraint based on the time between the first and last non-zero intensities during the IHIE (69 ± 13 μT recorded by samples 10017 and 10049 at 3,580 ± 9 Ma (refs. 1,55) and 54 ± 5 μT recorded by sample 10003 at 3,854 ± 8 Ma (refs. 50,55)). Second, the dynamo must have a maximum intensity of >53 μT, a constraint that is based on the highest lower limit on the strength of the palaeointensity (69 ± 13 μT recorded by samples 10017 and 10049[1]). Third, a period of dynamo activity must last at least 100 days ($2.7 \times 10^{-4}$ ka) to be captured during cooling of a typical lunar basalt, according to petrographic observations that suggest typical cooling rates between 0.5 and 100 °C $hr^{-1}$ from a temperature of 1,250 °C (refs. 37,38). Fourth, the dynamo must be active for at least 1% of the time throughout the IHIE based on a simple probability model outlined below.

The record is divided into discrete observations ($n$) covering the duration of basaltic volcanism and the entire palaeomagnetic record (Supplementary Fig. 7). Each sample is treated as a separate event, with events also grouped by geochronological age as summarized in Supplementary Table 1. For each case, we calculate the number of observations showing a positive field ($k$) on the basis of whether palaeointensity values are (or are not) within uncertainty of zero, and separately whether they are (or are not) within uncertainty of <20 μT. The corresponding $n$ and $k$ values for each scenario are provided in Supplementary Table 5.

We calculate the probability, $P$, that $k$ positive intensities are captured for $n$ discrete periods while varying the proportion of time the dynamo was active for, $p$, between 0 and 100% using

$$P(X \geq k) = 1 - P(X < k) \tag{3}$$

where

$$P(X < k) = \sum_{k=0}^{k} \binom{n}{k} p^k (1-p)^{n-k} \tag{4}$$

in the cases where $n > k$, and

$$P(X = k) = \binom{n}{k} p^k (1-p)^{n-k} \tag{5}$$

where $n = k$. In all cases

$$\binom{n}{k} = \frac{n!}{k!\,(n-k)!} \tag{6}$$

We then conservatively calculate the proportion of time the dynamo would need to be active for there to be a 1% chance ($P = 0.01$) of capturing the observed palaeomagnetic record (based on chosen values of $n$ and $k$; 1% is our tail probability). An example probability distribution is shown in Supplementary Fig. 8, where $n = 3$, $k = 3$ and a dynamo must be active for at least 22% of the time ($p = 0.22$) for there to be a 1% chance of observing three positive events. In this case, Apollo samples from the IHIE represent three discrete periods (Supplementary Fig. 7).

For all considered cases, we find for $P = 0.01$, the dynamo must be active for between 1 and 27% of the time ($p = 0.01$ to $p = 0.27$). Our modelling results cannot fulfil this criterion for any of the chosen values. We argue that the most realistic estimate is when we consider only basalts that acquired remanence during the IHIE. These samples fall into at least three discrete periods ($n = 3$) based on recent U–Pb ages[55], and palaeointensities exceeding 20 μT are recovered for each period ($k = 3$). However, if we consider that these basalts may have erupted more continuously throughout the IHIE, with larger uncertainties associated with each age[56,57], then the IHIE may represent only one

discrete period ($n = 1$). In this case, the dynamo is required to be active for only 1% of the time to generate one observation of a positive palaeointensity. It is important to note that at the boundary $n = 1, P(X \geq 1) = p$ imposing $P(X \geq 1) = 0.01$ states only that the dynamo must have been active long enough to yield a 1% chance of observing one positive event while it was operating. In this boundary case, where the IHIE is treated as a single event, our result is a conceptual limit under the imposed (conservative) tail probability, not a physical lower bound on $p$. Lower true dynamo activity timescales are possible but would make capturing this dynamo in a single sample correspondingly even less probable. Nonetheless, because this is the smallest inferred active fraction consistent with our chosen 1% significance threshold, we adopt it for comparison with modelling results, both for consistency and to emphasise that, regardless of how the palaeomagnetic record is interpreted, it remains highly unlikely to capture such rare, short-lived high-intensity dynamo events.

### A dynamo driven by protracted mantle overturn

Following Evans and Tikoo[29], we allow multiple Ti-rich diapirs with a maximum diameter of 40 km (the limit for which diapirs can become entrained by mantle convection[29]) to stochastically fall to the CMB where they melt over varying timescales. Diapir descent and melting continues until the total volume of Ti-rich material residing at the CMB implied by seismic observations is reached ($5.2 \times 10^8$ km$^3$) (ref. 58). By varying the number, size and frequency of Ti-rich diapirs sinking to the CMB, and their subsequent melting times, this simple model can produce synthetic surface magnetic fields as a function of time that can be compared with the observational record (Supplementary Fig. 9).

We allow multiple, spherical diapirs to fall to the CMB. Diapirs are sampled from a one-tailed, normal distribution with a maximum value of 40 km, and we investigate the effect of varying the standard deviation (the likelihood of sampling a large versus small diapir) in our results. The number of diapirs that can fall simultaneously is also varied as part of our simulations, with an upper limit fixed by the amount of ilmenite-bearing cumulate material at the CMB today (Supplementary Fig. 10). We explore three different regimes for the subsequent melting of diapirs. In the first regime, melting is proportional to the thickness of the ilmenite-bearing cumulate layer at the CMB. In the second regime, melting is proportional to the size of the largest diapir sinking in a single time step. In the third regime, melting time is treated as an independent variable (Supplementary Information section 3.1 and Supplementary Fig. 11). Results from the third melting case are presented in Fig. 3.

We assume that all the energy available to drive the dynamo is a result of the increased heat flux out of the core due to the latent energy required to melt the Ti-rich diapirs. The latent energy, $E_L$, is given by

$$E_L = V_D \rho_D L \tag{7}$$

where $V_D$ is the volume of ilmenite-bearing cumulates that drop simultaneously to the CMB as diapirs, $\rho_D$ is the density of the diapir material, which we take to be 4,000 kg m$^{-3}$, and $L$ is the latent heat of fusion, 300 kJ kg$^{-1}$.

For each time step, we calculate the total volume of diapirs that have fallen to the CMB, and the resulting thickness of the ilmenite-bearing cumulate layer at the CMB, $H$, where the total volume of the core and the overlying ilmenite-bearing cumulates, $V_{tot}$, is given by

$$V_{tot} = V_D + V_C \tag{8}$$

where $V_D$ is the volume of diapir material at the CMB and $V_C$ is the volume of the core. Next we can calculate the volume-equivalent radius, $R_{tot}$, by assuming that diapirs are spherical such that

$$R_{tot} = \left(\frac{3}{4\pi} V_{tot}\right)^{\frac{1}{3}} \tag{9}$$

and finally we calculate the height, $H$, using

$$H = R_{tot} - R_c. \tag{10}$$

The heat flux, $Q_{CMB}$, is given by

$$Q_{CMB} = \frac{R_D^3 \rho_D L}{3 R_C^2 \Delta t} \tag{11}$$

where $R_D$ is the radius of the total volume of Ti-rich cumulates dropped in one time step (assuming a spherical geometry), $R_C = 350$ km is the radius of the core, and $\Delta t$ is the melting time of the diapirs. For the first melting case, melting time is proportional to the thickness, $H$, of cumulates deposited at the CMB in a single time step, $\Delta t_c = cH$, where $c$ is a constant of proportionality, the value of which is varied. In the second melting case, melting time is proportional to the maximum individual diapir volume, $V_D^{max}$, that reaches the CMB in a single time step, $\Delta t_c = cV_D^{max}$. In the third case, melting time is independent of diapir volume and is varied as a free parameter where $\Delta t_c = c$.

The strength of the field generated at the surface, $B_S$, is approximated as

$$B_S \cong 2 \times 10^{-5} f_{dip} (Q_{CMB})^{\frac{1}{3}} \tag{12}$$

where the constant $2 \times 10^{-5}$ and $f_{dip} = \frac{1}{7}$, the proportion of the field that is dipolar, are based on dynamo scaling laws[11,59]. We allow diapirs to drop until the total volume of ilmenite-bearing cumulates thought to be present above the CMB today ($520 \times 10^6$ km$^3$) is exhausted, creating a cumulate layer with a thickness of 200 km (ref. 58).

We vary the maximum number of simultaneous diapirs that can fall, $D_{max}$, the shape of the normal, one-tailed distribution from which the size of the diapirs is taken, $D_{size}$, the duration of 'off' periods, when no diapirs drop to the CMB, $t_{off}$, and the constant of proportionality, $c$, between the melting time and the height of the Ti-rich cumulate layer at the CMB.

### A dynamo driven by melting of ilmenite-bearing cumulates at the CMB after mantle overturn

Following the mechanism proposed by Stegman et al.[30], ilmenite-bearing cumulates at the CMB heat up due to the presence of radiogenic elements within KREEP material. Once the cumulates become hot enough, they produce buoyant, Ti-rich melts that are re-entrained into the overlying mantle at the onset of convection around 3.9 Ga, consistent with the onset of the IHIE[33,47]. In this model, the heat flux across the CMB is elevated by the latent heat of cumulate melting (equation (7)). While the heat flux is likely to also increase due to the adiabatic removal of buoyant cumulate material, we contend this factor is probably not important given the large volume of ilmenite-bearing cumulates inferred at the CMB today[10,27] and the relatively small volume of high-Ti basalts on the lunar surface (~$1.8 \times 10^6$ km$^3$) (refs. 60,61). We assume that melting will introduce Rayleigh–Taylor instabilities, causing the melt to rise and temporarily elevate the heat flux across the CMB. While some melt will then erupt as high-Ti basalts, the majority will cool and crystallize as the temperature gradient re-equilibrates and sink back to the CMB where the process can repeat.

We consider upper and lower limits for the volume of molten ilmenite-bearing cumulates and use these to estimate the melting time that can produce the observed magnetic-field strengths. First, we calculate an upper limit by assuming that the entire cumulate layer at the CMB melts, but only a small amount of melt (<0.3%) becomes

sufficiently buoyant to reach the surface as high-Ti basalts. Second, we calculate a lower limit by assuming that only the volume of high-Ti basalts observed at the surface today melted and that melt extraction was 100% efficient.

We assume that all the ilmenite-bearing cumulates are at the CMB before the onset of the IHIE, and they can melt partially or entirely multiple times over. We use the relationship between surface field and volume (Equations (11) and (12)) to calculate upper estimates for melt time for the given surface magnetic-field intensities. Melting must fulfil our criterion of creating surface magnetic-field intensities that exceed 40–53 μT to explain the three high-intensity episodes recorded by high-Ti basalts (Fig. 1).

## Data availability

All data used in this paper are summarized in the Supplementary Tables 1–5 and are available via Zenodo at https://doi.org/10.5281/zenodo.18156520 (ref. 62). The data required to recreate Figs. 1–4 and Supplementary Figs. 1–11 are available via GitHub at https://github.com/TinySpaceMagnet/LunarDynamo (ref. 63).

## Code availability

All related Python code used in this study, including example code outputs (which are stochastic in nature), is available via GitHub at https://github.com/TinySpaceMagnet/LunarDynamo (ref. 63)

## References


49. Shea, E. K. et al. A long-lived lunar core dynamo. *Science* **335**, 453–456 (2012).
50. Jung, J.-I., Tikoo, S. M. & Burns, D. Assessing lunar paleointensity variability during the 3.9–3.5 Ga High Field Epoch. *Earth Planet. Sci. Lett.* **638**, 118757 (2024).
51. Nichols, C. I. O. et al. The palaeoinclination of the ancient lunar magnetic field from an Apollo 17 basalt. *Nat. Astron.* **5**, 1216–1223 (2021).
52. Cournède, C., Gattacceca, J. & Rochette, P. Magnetic study of large Apollo samples: possible evidence for an ancient centered dipolar field on the Moon. *Earth Planet. Sci. Lett.* **331–332**, 31–42 (2012).
53. Meyer, C. *The Lunar Sample Compendium* (NASA, 2008); http://curator.jsc.nasa.gov/lunar/lsc/
54. Gattacceca, J. et al. Can the lunar crust be magnetized by shock: experimental groundtruth. *Earth Planet. Sci. Lett.* **299**, 42–53 (2010).
55. Snape, J. F. et al. The timing of basaltic volcanism at the Apollo landing sites. *Geochim. Cosmochim. Acta* **266**, 29–53 (2019).
56. Snyder, G. A., Lee, D. C., Taylor, L. A., Halliday, A. N. & Jerde, E. A. Evolution of the upper mantle of the Earth's Moon: neodymium and strontium isotopic constraints from high-Ti mare basalts. *Geochim. Cosmochim. Acta* **58**, 4795–4808 (1994).
57. Paces, J. B. et al. A strontium and neodymium isotopic study of Apollo 17 high-Ti mare basalts: resolution of ages, evolution of magmas, and origins of source heterogeneities. *Geochim. Cosmochim. Acta* **55**, 2025–2043 (1991).
58. Khan, A., Connolly, J. A. D., Pommier, A. & Noir, J. Geophysical evidence for melt in the deep lunar interior. *J. Geophys. Res. Planets* **119**, 2197–2221 (2014).
59. Christensen, U. R., Holzwarth, V. & Reiners, A. Energy flux determines magnetic field strength of planets and stars. *Nature* **457**, 167–169 (2009).
60. Needham, D. H. & Kring, D. A. Lunar volcanism produced a transient atmosphere around the ancient Moon. *Earth Planet. Sci. Lett.* **478**, 175–178 (2017).
61. Giguere, T. A., Taylor, G. J., Hawke, B. R. & Lucey, P. G. The titanium contents of lunar mare basalts. *Meteorit. Planet. Sci.* **35**, 193–200 (2000).
62. Nichols, C. I. O., Wade, J. & Stephenson, S. N. An intermittent lunar dynamo linked to high-titanium volcanism on the Moon. *Zenodo* https://doi.org/10.5281/zenodo.18156520 (2026).
63. Nichols, C. I. O., Wade, J. & Stephenson, S. N. Lunar dynamo. *GitHub* https://github.com/TinySpaceMagnet/LunarDynamo (2026).


## Acknowledgements

We thank S. Tikoo for constructive feedback on this work. O. Lu and J. Ryan contributed to preliminary modelling.

## Author contributions

C.I.O.N conceived the idea in discussion with J.W. All relevant existing literature data were compiled by C.I.O.N. Heat flux modelling and statistical analyses were performed by C.I.O.N. and S.N.S. All authors contributed to the writing of the final manuscript.

## Competing interests

The authors declare no competing interests.

## Additional information

**Supplementary information** The online version contains supplementary material available at https://doi.org/10.1038/s41561-026-01929-y.

**Correspondence and requests for materials** should be addressed to Claire I. O. Nichols.

**Peer review information** *Nature Geoscience* thanks Alexander Nemchin and Sonia Tikoo for their contribution to the peer review of this work. Primary Handling Editor: Alison Hunt, in collaboration with the *Nature Geoscience* team.

**Reprints and permissions information** is available at www.nature.com/reprints.